Mapping the texture of plant protein blends for meat analogues

Floor K.G. Schreuders [a], Leonard M.C. Sagis [b], Igor Bodnár [c], Philipp Erni [c], Remko M. Boom [a], Atze Jan van der Goot [a],*

[a] *Laboratory of Food Process Engineering, Wageningen University, Bornse Weilanden 9, 6708, WG, Wageningen, the Netherlands*
[b] *Laboratory of Physics and Physical Chemistry of Foods, Wageningen University, Bornse Weilanden 9, 6708, WG, Wageningen, the Netherlands*
[c] *Firmenich S.A., Rue de La Bergère 7, CH-1242 Satigny, Geneva, Switzerland*

ARTICLE INFO

ABSTRACT

The development of next-generation meat analogues can be accelerated by in-depth knowledge of the rheological properties of dense biopolymer blends. Blends comprising plant proteins such as pea protein isolate or soy protein isolate combined with wheat gluten can be used to create a wide range of structures. The objective of this study is to demonstrate the use of texture maps to systematically show the rheological properties of plant proteins under conditions relevant to processing of meat analogue products. The first texture map was constructed by plotting the stress and strain at the end of the linear viscoelastic regime of the strain sweeps and a second map was based on the stress and strain at the crossover point of those sweeps. Next, a colour scheme was used to visualize the relative importance of the viscous and elastic contributions as a function of the strain amplitude and different ratios of each protein in the blend. The maps and schemes showed that heating induced elasticity. In pea protein–wheat gluten blends, lower strain, stress and elasticity values were obtained for pea compared with wheat gluten. In soy protein–wheat gluten blends, the texture properties were almost similar for the two components. Soy protein–wheat gluten blends are tougher and more elastic than pea protein–wheat gluten blends.

1. Introduction

Despite recent progress, meat analogues still differ from genuine meat in terms of mouthfeel, texture, taste and flavour (Samard & Ryu, 2019). Therefore, more insight is needed into the functionalities of plant proteins to transform them into materials with even better meat-resembling properties. Rheology can be used to characterize plant protein blends with regard to their functionality for use in meat analogue applications. Meat analogues often contain ingredients derived from soy, wheat or pea, and blends comprising these plant proteins can be used to create a wide range of structures (Bashi, McCullough, Ong, & Ramirez, 2019; Jones, 2016). Recent research revealed that fibrous structures were successfully created from pea protein isolate (PPI)–wheat gluten (WG) blends and soy protein isolate (SPI)–WG blends (Grabowska, Tekidou, Boom, & van der Goot, 2014; Schreuders et al., 2019). High moisture extrusion cooking of these ingredients is generally done with a dry matter content between 30 and 50 wt%, maximum temperatures between 100 °C and 170 °C, and short residence times (2–5 min) (Cornet et al., 2021). Structure formation processes of plant protein blends involve large deformations of the materials. Recently, it

was found that a closed-cavity rheometer used in the rubber industry allows accurate determination of the rheological properties of concentrated plant-based protein materials under extrusion relevant conditions (Dekkers, Emin, Boom, & van der Goot, 2018; Emin, Quevedo, Wilhelm, & Karbstein, 2017; Schreuders, Bodnar, Erni, Boom, & Goot, 2020). In a previous study, single ingredient dispersions (SPI, PPI and WG) were studied under conditions approaching the large-shear conditions relevant for structuring during heating and cooling (Schreuders et al., 2021). Here, we extend these analyses to blends of PPI–WG and SPI–WG with different protein ratios in the blends (20/80, 50/50, 80/20). Measurements of these protein blends under different processing conditions and ratios lead to a large amount of experimental data, but the data do not naturally lead to straightforward insights. Therefore, we propose the use of texture maps and colour schemes to provide overviews of a broad set of rheological measurements.

The starting point of the study is the use of large amplitude oscillatory shear (LAOS) measurements to characterize viscous and elastic properties under conditions relevant for structuring processes. LAOS provides insight into the non-linear response because the modulus depends on the applied strain and strain rate amplitude. For a large

---

* Corresponding author.
  E-mail address: atzejan.vandergoot@wur.nl (A.J. van der Goot).

amplitude sinusoidal strain input, the shape of the resulting stress waveform often deviates from a sinusoidal wave, with a significant contribution from higher-order harmonics. The LAOS information is typically extracted using Fourier-transform based methods (Hyun et al., 2011). Lissajous curves are used to facilitate the interpretation of a broad set of complex measurements. The so-called test space of the Lissajous curves is formed by two key parameters of LAOS deformation: frequency and strain amplitude. This test space is often shown in a Pipkin plot (Ewoldt & McKinley, 2017; Pipkin, 1972; Szopinski & Luinstra, 2016; Zhou, Cook, & McKinley, 2010). To better quantify the transitions in non-linear behaviour, the energy dissipation ratio was calculated and presented by colour contours in the Pipkin plot (Ewoldt, Hosoi, & McKinley, 2008; Tao et al., 2019). The energy dissipation ratio (ϕ) as proposed by Ewoldt et al. (2008) and Ewoldt, Winter, Maxey, and McKinley (2010) is the ratio between the actual dissipated energy and the dissipation of a material showing perfect plastic behaviour. When $\phi = 0$, the rheological response is purely elastic, while $\phi = 1$ implies that the material displays perfect plastic (Ptaszek, 2014). A ϕ of $\pi/4$ corresponds to a material that behaves as a Newtonian liquid. Texture maps provide a compact overview of the rheological properties for any material of interest. They summarize non-linear rheological information into two-dimensional plots involving only characteristic key parameters. This allows us to map the non-linear rheological behaviour of a great number of samples in an intuitive way. Fig. 1 exemplifies this approach and includes stress and strain values from previous studies. Although different parameters can be chosen for these plots, most texture maps are based on the stress and strain at the end of the linear viscoelastic (LVE) regime to classify products into four quadrants (Fig. 1) (Hamann & MacDonald, 1992). Materials in quadrant 1 on the lower left, with low shear stress and shear strain, are classified as a soft, non-shaped texture commonly referred to as "mushy" (such as for grits and similar food materials). Materials in quadrant 2 on the lower right, with low shear stress and high shear strain, are often described as "rubbery" (such as gelatin). Quadrant 3 on the top right, with strong materials with high shear stress and shear strain that are not easily broken, indicates a "tough" texture (for example, fruit leather and dried fruits). Quadrant 4 on the top left, with delicate and easily broken materials with high shear stress and low shear strain, clusters products with a "brittle" texture (such as many baked or confectionery food products; Tunick & Van Hekken, 2010). Although the texture of food can be considered as a sensory property related to the human response, it is also often measured instrumentally in terms of mechanical or rheological proprieties (Altay & Gunasekaran, 2013). The latter study relate "texture" and used texture maps for instrumental responses such as the shear stress and strain at failure and classify those responses as rubbery, mushy, brittle and tough.

Good examples of this approach are available for cheese (Truong & Daubert, 2001), soybean protein (tofu) and gellan gum gels (Truong & Daubert, 2000), cross-linked waxy maize, tapioca, and Amioca starch dispersions (Genovese & Rao, 2003), mixed gelatine/SPI gels (Ersch, ter Laak, van der Linden, Venema, & Martin, 2015) and heat-induced PPI with microbial transglutaminase (Shand, Ya, Pietrasik, & Wanasundara, 2008).

The objective of this study is to map the rheological properties of plant protein blends under conditions relevant to meat analogue processing in a compact way using texture maps and colour schemes. In this article, three rheological parameters are mapped: stress at the end of the LVE regime and the stress–strain crossover point are captured in texture maps, and the energy dissipation ratio is demonstrated with colour schemes. The dissipation ratio is represented by colour contours in strain–protein ratio diagrams.

2. Materials and methods

2.1. Materials

PPI (NUTRALYS F85G) and vital WG (VITENS CWS) were both purchased from Roquette Frères S.A. (St. Louis, MO, USA). SPI (SUPRO EX 37 IP) was purchased from Solae (Europe S.A.). PPI was composed of 78.6 wt% protein (N × 5.7), WG was composed of 72.4 wt% protein (N × 5.7), SPI was composed of 80.0 wt% protein (N × 5.7) on a dry weight basis, according to Dumas measurements. The manufacturer's specifications indicated that the PPI contained 1 wt% dietary fibre, 9 wt% lipids, 4 wt% ash; SPI contained ≤1 wt% lipids, ≤5 wt% ash; and WG contained 10 wt% starch, 0.5 wt% cellulose fibre, 3 wt% lipids and 1 wt % ash. PPI, SPI and WG had an average dry matter content of 93.2 wt%, 92.8 wt%, and 92.3 wt%, respectively. Sodium chloride was obtained from Sigma-Aldrich (Zwijndrecht, the Netherlands).

2.2. Preparation of proteinaceous materials

Different ratios of protein were mixed (20/80, 50/50, 80/20) for the PPI–WG and SPI–WG blends. The sample preparation procedure has been described in detail previously by Grabowska et al. (2014). Protein blends (PPI, SPI, WG, PPI–WG and SPI–WG) were prepared with a final dry matter content of 40 wt% (Fig. 2). First, 1 wt% sodium chloride was dissolved in distilled water. Then the PPI, SPI and WG materials were prepared by dispersing PPI, SPI or WG powder in the saline solution (at room temperature), followed by mixing by hand using a spatula until a homogeneous paste was obtained. The protein material was then hydrated at room temperature for 30 min and the material was covered
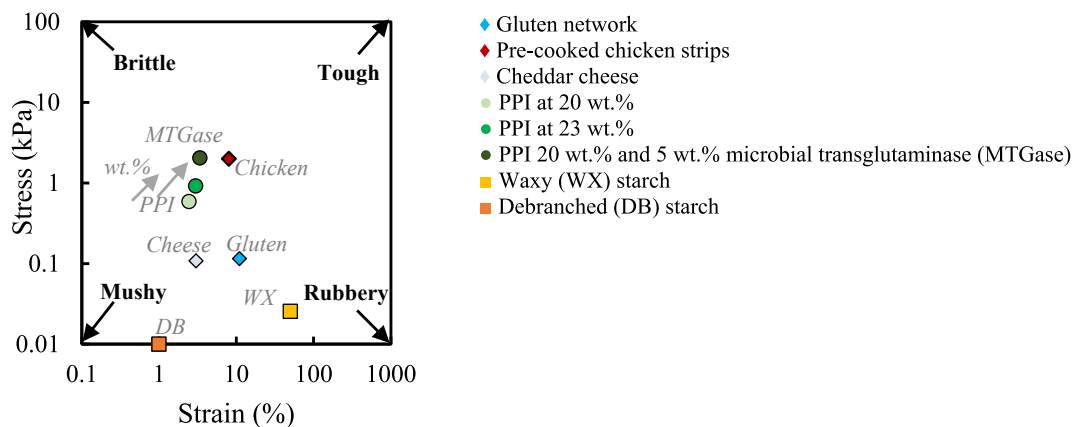

Fig. 1. A texture map plotting stress versus strain to classify food products into four quadrants. Texture map of different literature values at the end of the LVE regime was analysed for a gluten network, pre-cooked chicken strips and cheddar cheese at 50 °C and 0.48 Hz (Mattice & Marangoni, 2020), PPI at 20 wt%, 23 wt% and 20 wt% and 5 wt% microbial transglutaminase (MTGase) at 20 °C and 2 Hz (Moreno et al., 2020), waxy (WX) and debranched (DB) starch at 15 wt% at 20 °C and 0.16 Hz (Precha-Atsawanan, Uttapap, & Sagis, 2018).
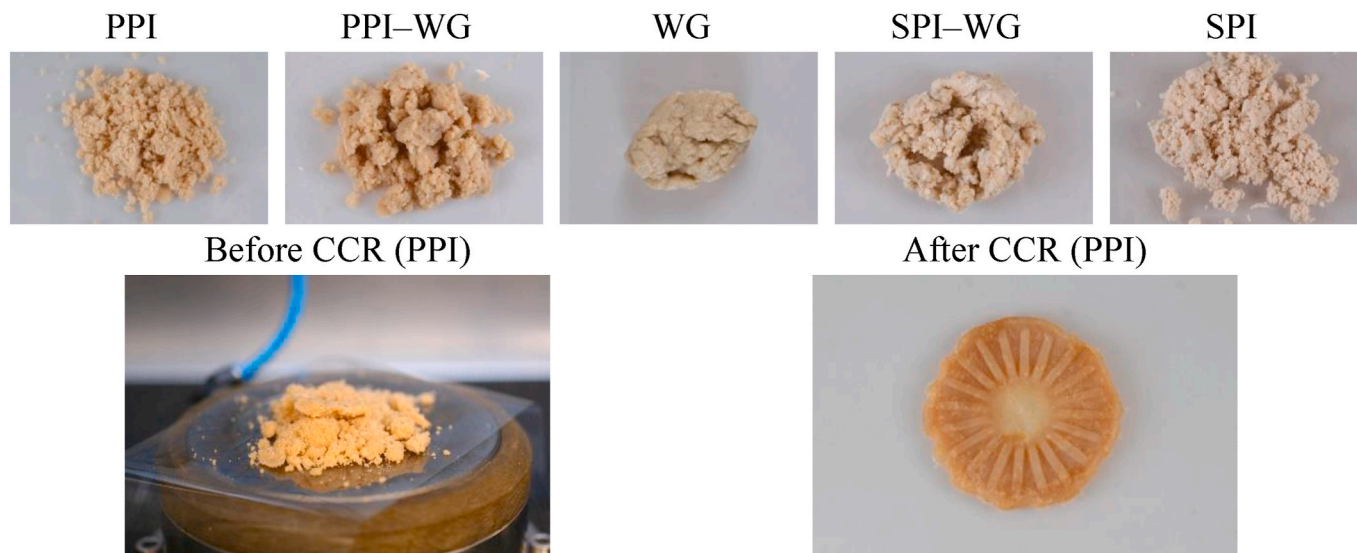
Fig. 2. Protein blends (PPI, SPI, WG, PPI-WG (50/50) and SPI-WG (50/50)) were prepared with a final dry matter content of 40 wt%. Pea protein blend with a moisture content of 40 wt% before (left) and after (right) a rheological measurement in a closed cavity rheometer.

with Parafilm (Pechiney Plastic Packaging, Chicago, IL, USA) to prevent water evaporation. For the PPI–WG and SPI–WG blends, the WG was mixed into the hydrated PPI or SPI dispersion with a spatula directly before the rheological measurement.

2.3. Rheological properties

The rheological properties of the protein materials were measured with a closed-cavity rheometer (CCR) (RPA Elite, TA instruments, New Castle, DE, USA) (Emin, Quevedo, Wilhelm, & Karbstein, 2017). Approximately 6 g was placed in between two plastic films in the closed cavity, which was sealed with a closing pressure of 4.5 bar to prevent water evaporation at high temperature. The transformation of pea protein dispersion into a solid mass can be observed in Fig. 2 before and after measurement in the CCR, suggesting a kind of melting of the particles during the measurement. The geometry of the CCR has a radius of 22.5 mm, maximum height of the inner cavity of 4 mm and a biconical opening with an angle of 3.35° for homogeneous transmission of the shear stress to the protein materials. The grooves on the surface of the cones prevent slippage. In this setup, the lower cone oscillates in strain-controlled mode while the upper cone remains stationary. First, the protein material was heated for 2 min at constant temperatures (i.e. 30 °C, 100 °C, 120 °C and 140 °C) without a shear treatment. Subsequently, strain sweep (0.01%–1000%) experiments were performed at these temperatures at a constant frequency (1 Hz). In a second type of test, the protein material was heated at constant temperatures (i.e. 30 °C, 100 °C, 120 °C and 140 °C) for 2 min and cooled to 30 °C at a cooling rate of 5 °C/min without shear treatment. After that, strain sweep experiments were performed at 30 °C at a constant frequency (1 Hz).

A strain sweep experiment is used to determine the yield stress and the flow stress of a material. The yield stress is defined as the value of the shear stress at the end of the LVE regime. Here, we define this stress as the point where G' differs more than 5% from its strain-independent value in the LVE regime (Fig. 3) (Nashif, Jones, & Henderson, 1985; Wereley et al., 2006). The flow stress is defined as the value of shear stress at the crossover point where the storage modulus is equal to the loss modulus ($G' = G''$).

2.4. Large amplitude oscillatory shear

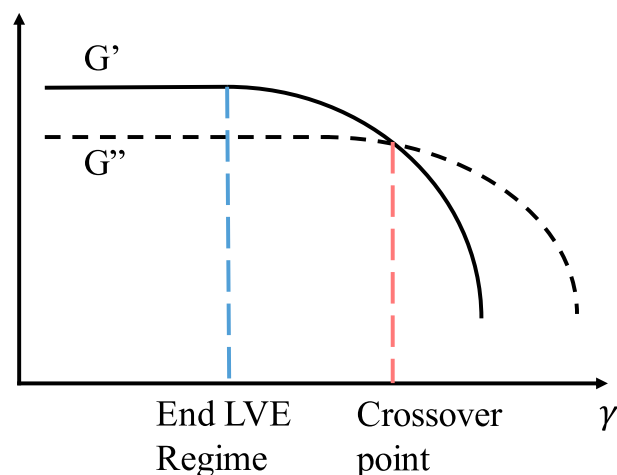The stress and strain data obtained from the LAOS measurements

Fig. 3. The storage modulus (G') and loss modulus (G'') versus strain. Vertical lines indicate the crossover point ($G' = G''$) and the end of the linear viscoelastic (LVE) regime (Wereley et al., 2006).

were analysed using the MITlaos software (version 2.1 beta, freeware distributed from MITlaos@mit.edu). The strain amplitude varied in the range of 0.01%–1000% at a constant frequency of 1 Hz at 30 °C. Lissajous curves were used to relate the response of the protein materials to the imposed oscillatory strain.

The area enclosed in a Lissajous curve is equal to the energy dissipated per unit volume during one complete cycle of the imposed oscillatory strain. The energy dissipated per unit volume in a single cycle is a function only of the first-order viscous Fourier coefficient (G_1''); calculated from the intensity and phase of the first-harmonic):

$$E_d = \oint \sigma d\gamma = G_1'' \gamma_0^2 \tag{1}$$

The energy dissipated by a perfectly plastic material in a single cycle is equal to

$$(E_d)_{pp} = 4\,\gamma_0 \sigma_{\max} \tag{2}$$

for a given strain amplitude (γ_0) and a maximum stress ($\sigma_{\max}$).

The ratio of the actual dissipated energy and the perfectly plastic

dissipation gives the energy dissipation ratio (ϕ) as proposed by Ewoldt et al. (2010).

$$\phi = \frac{E_d}{(E_d)_{pp}} = \frac{\pi G_1'' \gamma_0}{4\sigma_{max}} \qquad (3)$$

3. Results and discussion

3.1. Texture maps at the end of the LVE regime

Fig. 4 presents the texture map of the PPI–WG blends at ratios of 0/100, 20/80, 50/50, 80/20 and 100/0 at 30 °C, at high temperature (100 °C), and heating at 100 °C and cooling to 30 °C. At 30 °C, PPI materials generally became brittle, whereas WG materials were rubbery. A blend of PPI and WG yielded products with intermediate values in hardness and deformability. More PPI in a blend led to increased stress and reduced strain making the product more brittle. Those values are compared with the stress and strain values obtained from products depicted in Fig. 1. PPI at 40 wt% is tougher than at 20 wt% and 23 wt% PPI (Moreno et al., 2020). The texture properties of PPI (20 wt%) with 5 wt% transglutaminase are tougher compared with only PPI (20 wt%), which have texture properties similar to pre-cooked chicken strips (Mattice & Marangoni, 2020). Upon heating, PPI products changed to more mushy behaviour, whereas WG products became tough (as indicated by the grey arrow in Fig. 4). More PPI in a blend led to lower stress and strain, making the product mushier. The addition of WG led to higher stress and strain, making the product stronger, but also more stretchable. To summarize, upon heating, a shift in the texture map is observed compared with that at 30 °C from brittle to mushy for PPI and from rubbery to tough for WG. A similar shift was observed for blends heated at 120 °C and 140 °C (appendix Fig. A1). After heating and cooling, more PPI in a blend led to reduced stress and strain, making the product more mushy. More WG, however, resulted in an increase in the stress and strain, making the product tougher. A similar trend from mushy to tough texture upon higher WG content in the blend was observed when blends were heated at 120 °C and 140 °C and cooled to 30 °C (appendix Fig. A1). The strengthening of WG and PPI–WG blends after heating and cooling compared with those at 30 °C suggests the formation of additional physical interactions; for example, hydrogen bonding. PPI-only dispersions gave a lower stress and strain after the complete measurement, implying that the network is weakened; for example, a lower ability to form additional physical interactions during cooling.

We compared the behaviour of PPI–WG blends with that of SPI–WG blends. Fig. 4 presents a texture map of the SPI–WG blends at ratios of 0/100, 20/80, 50/50, 80/20, and 100/0. At 30 °C, SPI products were commonly brittle. The combination of SPI and WG yielded products with intermediate values in hardness and deformability. The SPI–WG products showed slightly higher stress values compared with PPI–WG

products. Heating SPI to 100 °C slightly transformed the material to rubbery behaviour (as indicated by the grey arrow in Fig. 4). The reduced stress observed in the texture maps of both PPI and SPI compared with 30 °C could be the effect of weakening of the physical interactions that stabilize the protein material, because the protein materials can now be considered as a melt. Heating WG resulted in tougher behaviour, whereas the SPI–WG blend gave slightly smaller strain values with higher SPI content, making the product less stretchable. An opposite trend was observed at higher temperatures (i.e. 120 °C and 140 °C) (appendix Fig. A1) and resulted in a higher strain for SPI and a lower strain for WG. The SPI–WG blend showed products with minimum values for stress and strain. For the SPI–WG blends, small differences were observed in the stress and strain values. This is on contrast to the outcomes with PPI–WG blends, where larger differences were observed in the stress and strain values between the components in the blend. After heating and cooling, both SPI and WG products have higher stress and strain compared with those at 30 °C and both show strengthening of the network, suggesting the formation of additional physical interactions. This is most pronounced for WG. After heating and cooling, the SPI–WG blend did not show products with intermediate values in hardness and deformability. This blend showed slightly higher stress compared with that at 30 °C and higher stress values compared with the PPI–WG blend.

The effect of temperature on both PPI–WG and SPI–WG blends at a 50/50 ratio is presented in a texture map in Fig. 5, at 30 °C, at high temperature (100 °C, 120 °C, 140 °C) and after heating at 100 °C, 120 °C, 140 °C and cooling to 30 °C. The plant protein blends heated to different temperatures covered a wide range of stresses and strains. Without heating, the stresses and strains of the SPI–WG and PPI–WG blends were similar. For the PPI–WG blends, heating at higher temperatures leads mainly to softer products, whereas, for the SPI–WG blends, heating leads to a tougher/rubbery character. After heating and cooling, both PPI–WG and SPI–WG products became tougher, meaning that heating resulted in a stronger material for the blends. This increase after 140 °C was also observed in a previous study in a tensile test at room temperature on PPI–WG product, sheared (39 s^{-1}) and heated (140 °C) in the shear cell (Schreuders et al., 2019). In general, the SPI–WG blends are tougher than the PPI–WG blends.

3.2. Texture maps at the crossover point

The texture properties at the crossover point of both the PPI–WG and SPI–WG blends are shown in Fig. 6. At 30 °C, PPI is characterized as brittle, whereas WG is characterized as rubbery. Combining PPI and WG in a blend yielded a lower intermediate crossover point in hardness and deformability. Heating made PPI products softer and WG products became less deformable. More PPI in a blend led to reduced crossover stress, whereas more WG in the blend led to increased crossover stress.
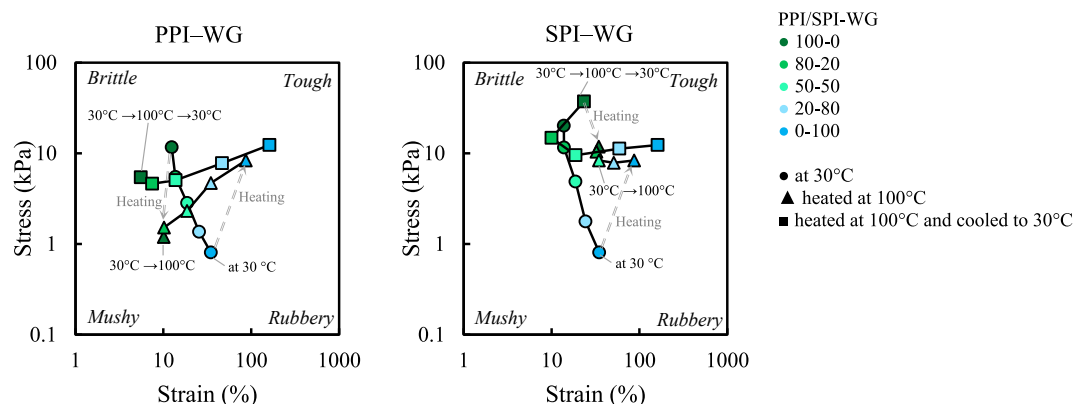

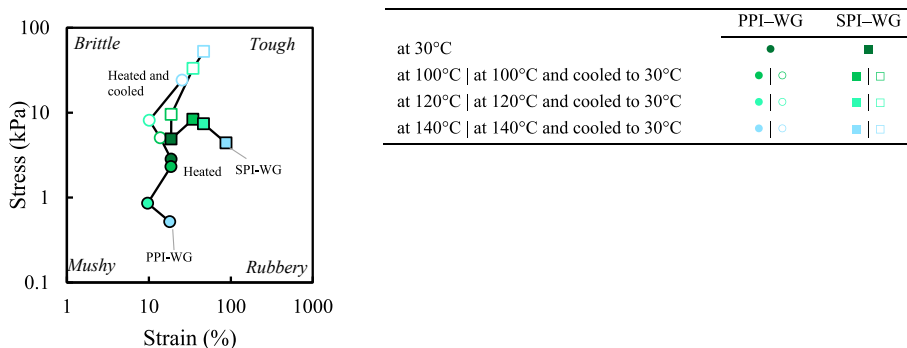**Fig. 4.** Texture map at the end of the LVE regime for PPI–WG and SPI–WG at 40 wt%. Lines are drawn for visual guidance.

	PPI–WG	SPI–WG
at 30°C	●	■
at 100°C | at 100°C and cooled to 30°C	● | ○	■ | □
at 120°C | at 120°C and cooled to 30°C	● | ○	■ | □
at 140°C | at 140°C and cooled to 30°C	● | ○	■ | □

Fig. 5. Texture maps at the end of the LVE regime of 40 wt%, 50/50 blend of PPI–WG and SPI–WG. Lines are drawn for visual guidance.
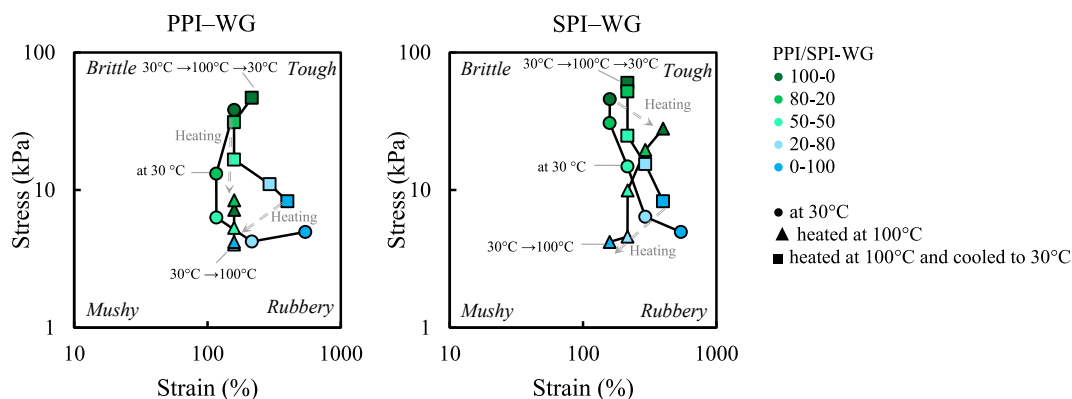

Fig. 6. Texture map at the crossover point of chicken and commercial meat analogues. Note that the scales of the x and y axes are different from those in Figs. 4, 5 and 6. Lines are drawn for visual guidance.

Heating to higher temperature resulted in a decreased stress for PPI (appendix Fig. A2). After heating and cooling, the PPI and WG materials became comparable with those at 30 °C, however, for WG a further increase in the temperature (i.e. 120 °C and 140 °C) resulted in larger crossover stress and smaller crossover strain (appendix Fig. A2).

SPI-based materials were commonly brittle, whereas WG materials were rubbery at 30 °C. With both SPI and WG, intermediate values in hardness and deformability were obtained in those products. Heating SPI shifted the crossover point to higher strain values and slightly lower stress values, whereas WG products became less deformable upon heating. Higher temperatures resulted in decreased stress for SPI. By combining SPI and WG in a blend, products with intermediate values in hardness and deformability were obtained. A further increase in the heating temperature (i.e. 140 °C) gave a smaller difference between the stress and strain values of SPI and WG (appendix Fig. A2). After heating and cooling, the SPI and WG products became comparable to those at

30 °C, however, increasing the temperature (i.e. 120 °C and 140 °C) resulted in increased stress of the crossover point for SPI and increased stress and decreased strain of the crossover point of WG (appendix Fig. A2).

A texture map for the crossover points is presented in Fig. 7 for both PPI–WG and SPI–WG blends at a 50/50 ratio at 30 °C, at high temperature (100 °C, 120 °C, 140 °C) and after heating at 100 °C, 120 °C, 140 °C and cooling down to 30 °C. At 30 °C, the crossover stress and strain values indicated that the SPI–WG blend became tough, whereas the PPI–WG blend became mushy. For both PPI–WG and SPI–WG blends, heating at higher temperatures led to reduced crossover stress, making the product softer. After heating and cooling, both PPI–WG and SPI–WG products had higher stress compared with those at 30 °C, meaning that heating resulted in a stronger material. After heating and cooling, the PPI–WG and SPI–WG blends at high temperatures resulted in higher stress, making both materials stronger. The results presented
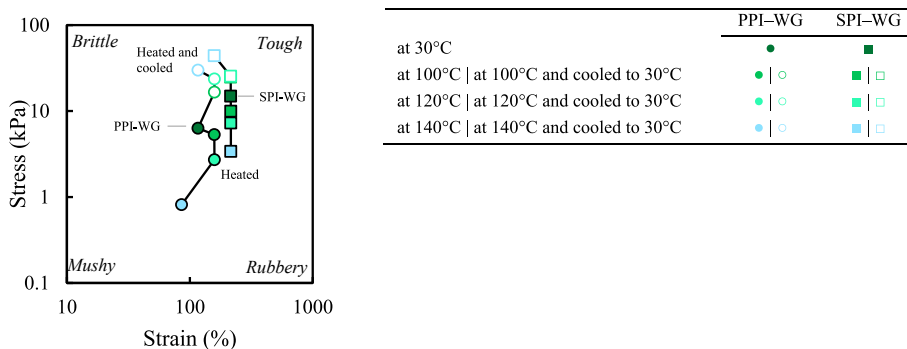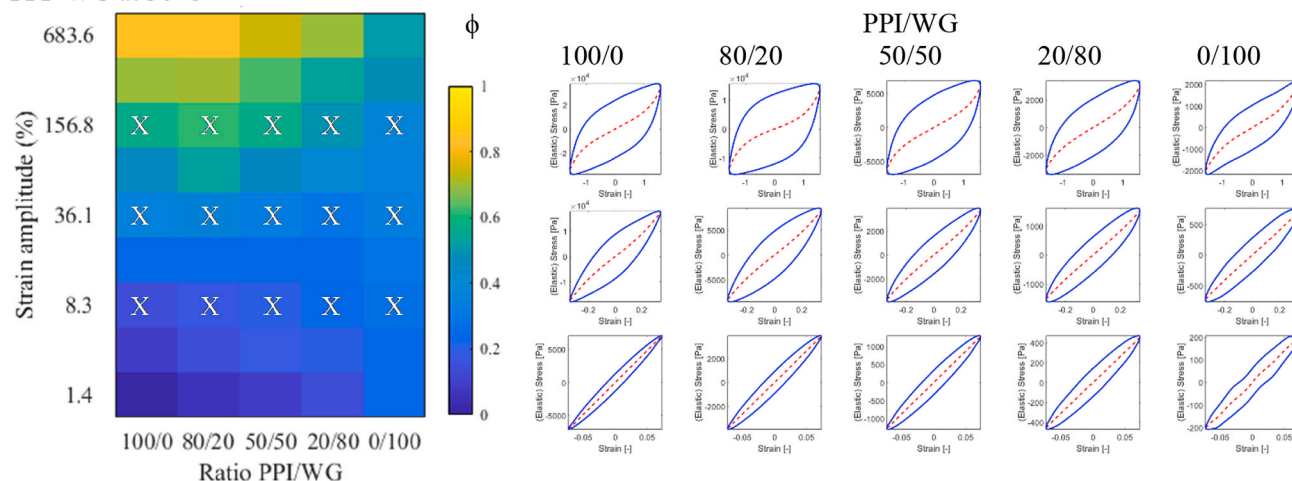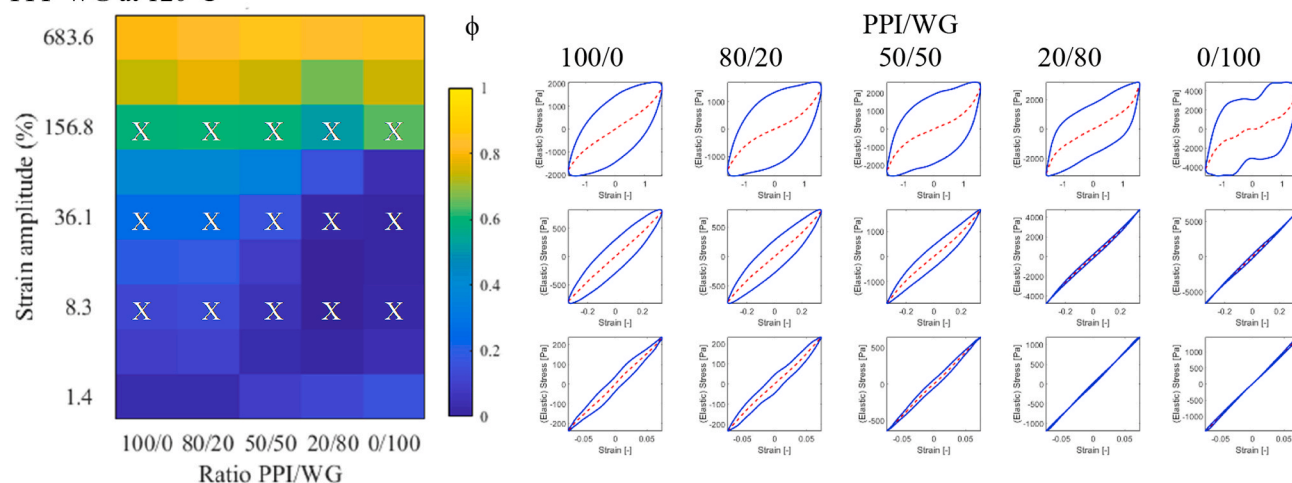

	PPI–WG	SPI–WG
at 30°C	●	■
at 100°C | at 100°C and cooled to 30°C	● | ○	■ | □
at 120°C | at 120°C and cooled to 30°C	● | ○	■ | □
at 140°C | at 140°C and cooled to 30°C	● | ○	■ | □

Fig. 7. Texture map at the crossover point of PPI–WG and SPI–WG at 40 wt%. Note that the scales of the x and y axes are different from those in Figs. 4, 5 and 6. Lines are drawn for visual guidance.
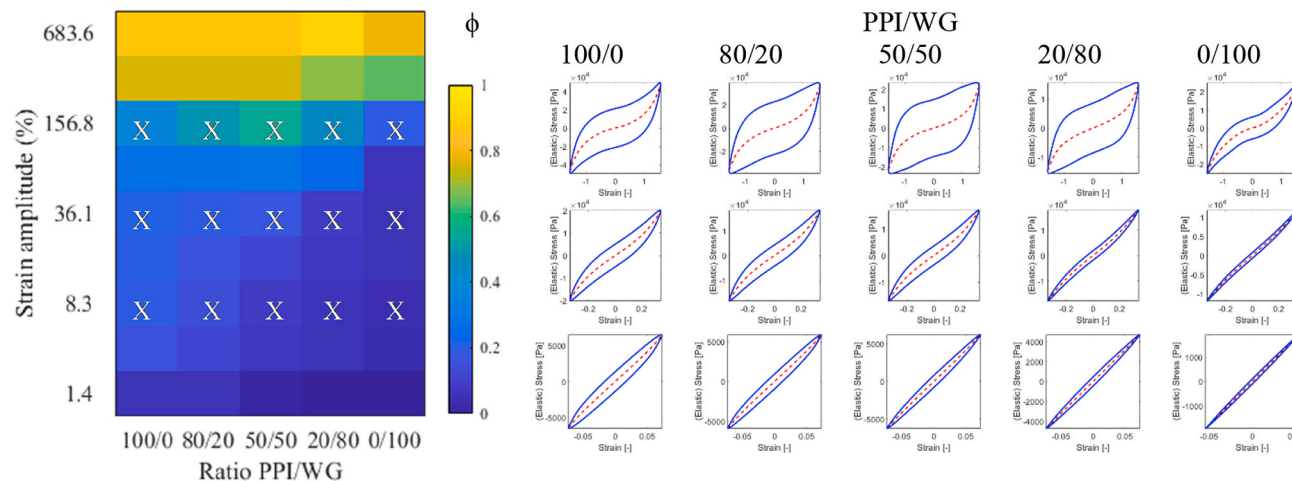
Fig. 8. Colour scheme of the dissipation ratio (φ) in a strain–protein ratio diagram for a PPI–WG and SPI–WG blend at different ratios at 30 °C, heated at 120 °C, and heated at 120 °C and cooled to 30 °C. The colour corresponds to the value of the dissipation ratio (φ) in the colour bar, φ = 0, elastic; φ = π/4, viscous; φ = 1, perfect plastic. The colour scheme of the dissipation ratio at increasing temperatures is shown in Video 1 (including heating at 100 °C and 120 °C and heated at 100 °C and 120 °C and cooled to 30 °C). Right: Lissajous curve of stress versus strain amplitude at three different strain amplitudes corresponding to the X symbol in the left panel (individual plots of normalized stress [solid lines] and elastic stress [dashed lines] vs. strain). (For interpretation of the references to colour in this figure legend, the reader is referred to the Web version of this article.)

SPI–WG at 30°C
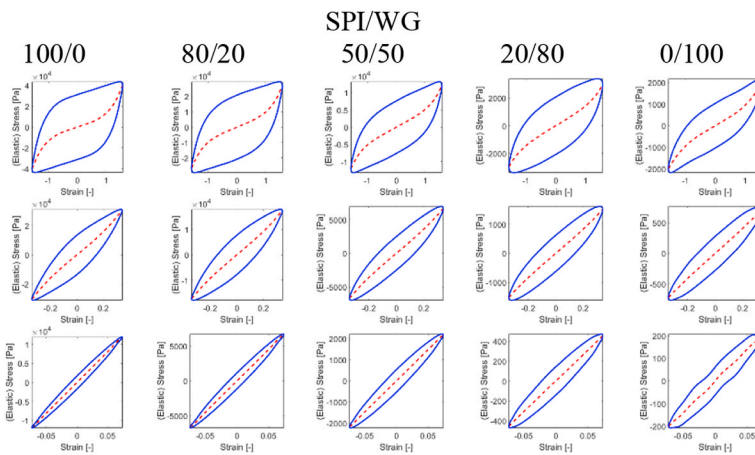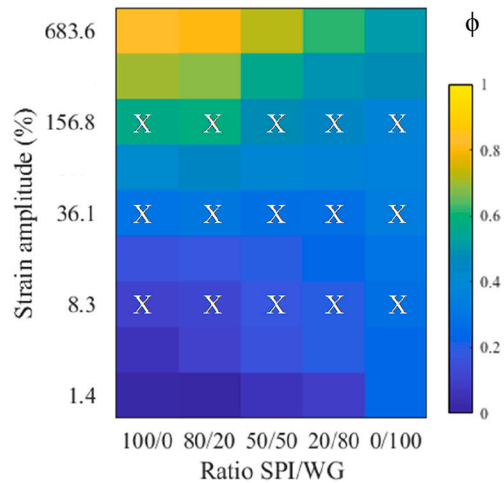
SPI–WG at 120°C
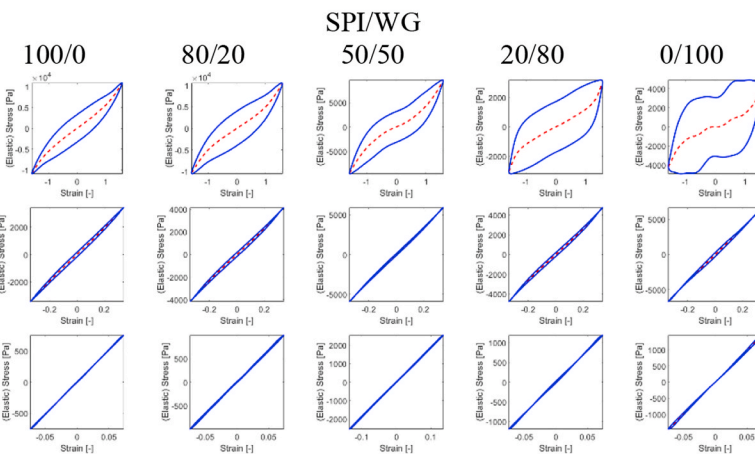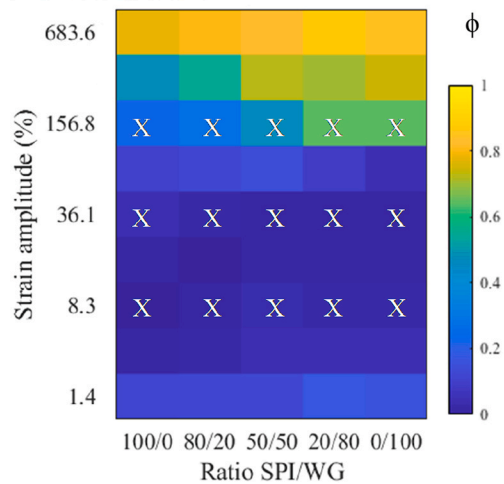
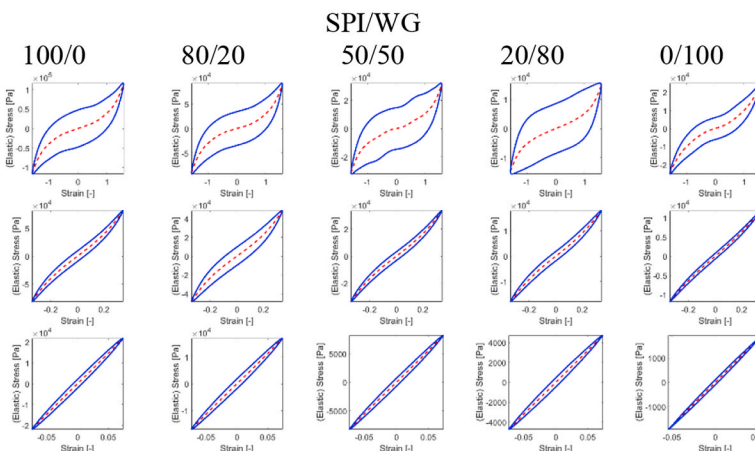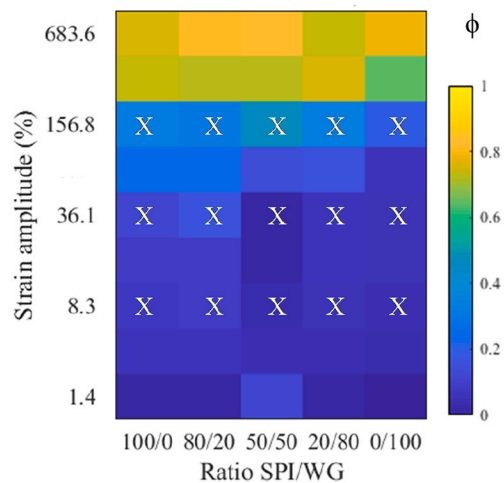## SPI–WG heated at 120°C and cooled to 30°C

Fig. 8. (*continued*).

Table 1

Summary of the texture maps and colour schemes presented in this paper (marked with an asterisk) after heating and cooling.

	Texture map		Colour scheme
	End of the LVE regime	Crossover point	Dissipation ratio
Difference between products*			
SPI–WG compared to PPI–WG	Tougher	Tougher	More elastic
Effect of heating*			
WG	Tougher	Slightly more brittle	More elastic
SPI	Slightly tougher	Slightly tougher	More elastic
PPI	Mushy	Slightly tougher	Slightly more elastic
SPI–WG	Stronger/tougher	Stronger/tougher	More elastic
PPI–WG	Stronger	Stronger/tougher	Slightly more elastic
Increased ratio of WG in the blend			
SPI–WG	Rubbery	Rubbery	–*
	Rubbery/more deformable*	Rubbery*	
PPI–WG	Rubbery	Rubbery	More elastic*
	Tougher*	Rubbery*	

here confirm that the SPI–WG blends are tougher than the PPI–WG blends.

3.3. Colour scheme to describe the dissipation ratio

A more detailed assessment of the non-linear viscoelastic behaviour of protein materials was obtained with Lissajous curves. The dissipation ratio was then calculated to summarize the essential non-linear behaviour (Ewoldt et al, 2008, 2010; Klost, Brzeski, & Drusch, 2020; Tao et al., 2019). The values are presented in a colour scheme to facilitate comparison. The left-hand panel of Fig. 8 shows these colour schemes for PPI–WG and SPI–WG. In the right-hand panel of Fig. 8, the corresponding elastic Lissajous curves are shown for the grid values of imposed strain amplitude and protein ratios marked by the crosses in the left-hand panel (colour scheme of the dissipation ratio). In the following, the dissipation ratios with increasing strain amplitudes of the PPI–WG and SPI--WG blends at ratios of 0/100, 20/80, 50/50, 80/20, and 100/0 (Fig. 8) are discussed. At 30 °C, PPI showed an increasing dissipation ratio for increasing strain amplitude. The elastic Lissajous curves had a line or narrow ellipse shape for small strain amplitudes, implying that the response of this material was mostly elastic at these strains. With a further increase in the strain amplitude, the area encompassed by the curve became wider. This is an indicator of increased viscous dissipation that allows the protein particles in the matrix to flow past each other, and eventually structure breakdown. The red dashed lines indicate the elastic contributions to the total stress. The dissipation ratio for increasing strain amplitudes remained constant for WG. The PPI–WG blend yielded products with intermediate dissipation ratios. At equal strain amplitude, more PPI in a blend gave a larger dissipation ratio. Heating WG lowered the dissipation ratios for almost all strain amplitudes and a more sudden transition to viscous behaviour. For WG, narrow ellipses were observed at low strain amplitude, indicating the predominant elastic behaviour. The dissipation ratio of PPI did not change upon heating, as indicated by only minor changes in the Lissajous curves of PPI. More PPI in the blend resulted in a gradual increase in the dissipation ratio for increasing strain amplitudes. Most PPI–WG blends yielded intermediate dissipation ratios. After heating and cooling, both PPI and WG became more elastic for a longer strain amplitude compared with the unheated materials. Again this abrupt transition in dissipation ratio for increasing strain amplitude was most pronounced for WG and also present in the blend containing a higher WG content.

We now compare the dissipation behaviour of PPI–WG blends with that of SPI–WG blends at different temperatures. The dissipation ratios of unheated SPI–WG and PPI–WG blends at ratios of 20/80, 50/50 and 80/20 were comparable. SPI only showed a larger dissipation ratio for increasing strain amplitudes. Both SPI–WG and PPI–WG blends resulted in products with intermediate dissipation ratios. Heating led to lower dissipation ratios for SPI, WG and SPI–WG blend and resulted in similar elastic behaviour in the case of the SPI–WG blend for different protein ratios. In the Lissajous curves, narrow ellipses were observed at low strain amplitude, indicating the predominant elastic behaviour. Extensive deformation led to a sudden onset of viscous/plastic behaviour. After heating and cooling, both SPI and WG became more elastic across a wider range of strain amplitudes compared with untreated materials. The SPI–WG blend (50/50) showed lower dissipation ratios (~36% strain amplitude) compared with SPI and WG at similar strain amplitude, indicating increased elasticity. That could indicate synergetic effects between SPI and WG, indicative of specific interactions.

3.4. Combining texture maps and colour schemes to describe the dissipation ratio

Texture maps give an efficient and quantitative summary that give food product development teams and process engineers insight into the effects of ingredients and processing conditions on the material properties relevant to product texture. Table 1 gives an overview of all the results presented in the texture maps and colour schemes. Both maps revealed that SPI–WG is tougher than PPI–WG and that an increase in WG in the blend resulted in a more rubbery material. Similar differences between the protein materials were described in previous studies even though a much lower protein concentration (~10 wt%) was investigated than the concentration commonly used in high moisture extrusion cooking (>30 wt%). As observed in previous studies, PPI forms weaker and less elastic gels compared with SPI (Batista, Portugal, Sousa, Crespo, & Raymundo, 2005; Lam, Can Karaca, Tyler, & Nickerson, 2018; O'Kane, Happe, Vereijken, Gruppen, & Van Boekel, 2004). Batista et al. (2005) established a relationship between a stronger gel and more protein unfolding during and after thermal treatment. After protein unfolding, protein aggregates are formed through hydrophobic interactions and strengthened further due to the formation of disulphide bridges. The total number of cysteine residues differs between types of protein and the number of potential disulphide bonds that can be formed. The accessibility of free thiol groups and disulphide bonds are both important to network formation. Gluten contains relatively large amounts of cysteine (Shewry & Tatham, 1997), whereas pea protein contains relatively low amounts.

Also, differences between the texture maps were observed. The effect of heating was observed differently in both maps. When comparing the texture map at the end of the LVE regime with the texture map at the crossover point, we actually compare the effect of small strain in the LVE regime and larger strain in the non-linear regime. At small strains, the material is deformed more after heating and cooling, making the material mushier for PPI. However, WG became a tougher material. This could be related to weakening of the physical interaction for PPI and the formation of additional physical interactions for WG upon heating. At larger strains, at the crossover point in the texture map, both the

temperature and strain amplitude will influence the material. At larger strain, the protein aggregates in the matrix start to flow past each other. Heating and cooling transformed PPI into a slightly tougher product and WG into a more brittle product. This texture map in the non-linear region is especially interesting for shear-induced structuring where the material is sheared beyond the linear regime. The linear and non-linear regimes also explain the different response of the protein materials after heating. Therefore, we conclude that analysing the combination of the two texture maps is important.

The texture of plant-based protein products is influenced by both composition and process conditions. The main question is the mechanisms underlying the differences in stresses and strains of the blends. Two different situations can be observed in the texture maps:

1. A blend gives intermediate hardness and deformability, and intermediate values in stress and strain values. Heating PPI makes the blend weaker and less deformable, whereas WG increases the strain and stress making the gels tougher. For PPI–WG blends, the end of the LVE regime was observed in the blend with intermediate values in hardness and deformability of PPI and WG. Similarly for non-linear rheology, intermediate dissipation ratio values were observed.
2. Blends yield intermediate values in hardness and deformability but minimum stress and strain values. For SPI–WG, this behaviour was observed in the texture maps. We hypothesize that this could be due to phase inversion, the point in the texture map where blend components exchange their discontinuity. The blend with low WG content is SPI continuous. As the WG content increases in the blend, a continuous WG network is formed or a bi-continuous WG network that is entrapping the SPI network. In the dissipation ratio maps, a lower dissipation ratio was observed in the blend compared with the single components, which indicated increased elasticity in the blend. Furthermore, the stress and strain values of SPI and WG in the SPI–WG blend are closer together in the texture and dissipation maps, whereas the PPI and WG phases in the PPI–WG blend show a distinct difference.

4. Conclusion

The rheological properties of SPI, PPI and blends of these with WG were quantified using texture maps and dissipation ratios obtained from large-deformation Lissajous curves. Different composition and processing conditions were investigated. We showed that the three rheological parameters, (1) stress at the end of the LVE regime, (2) the stress–strain crossover point and (3) the dissipation ratio, provide a useful rheological fingerprint of these food products and materials.

As observed in the maps and schemes, heating induced more elasticity. In PPI–WG blends, PPI has lower strain, stress, and elasticity compared with WG. In SPI–WG blends, the texture properties are almost similar for the two components. SPI–WG blends are tougher and more elastic compared with PPI–WG blends. Mapping the rheological properties at the end of the LVE regime, the crossover point as well as the dissipation ratio as a function of small and large strain amplitudes, is useful for further understanding and use of dense protein blends.

CRediT author statement

Floor K. G. Schreuders: Investigation, Writing - Original Draft, Writing - Review & Editing; Leonard M.C. Sagis – Writing - Review & Editing; Igor Bodnár: Writing - Review & Editing; Philipp Erni: Writing - Writing - Review & Editing; Remko M. Boom: Supervision, Writing - Review & Editing; Atze Jan van der Goot (*corresponding author): – Supervision, Writing - Review & Editing

Declaration of competing interest

The authors report no conflicts of interest relevant to this article.

Appendix A. Supplementary data

Supplementary data to this article can be found online at https://doi.org/10.1016/j.foodhyd.2021.106753.

References

Altay, F., & Gunasekaran, S. (2013). Gelling properties of gelatin – xanthan gum systems with high levels of co-solutes. *Journal of Food Engineering, 118*(3), 289–295. https://doi.org/10.1016/j.jfoodeng.2013.04.018

Bashi, Z., McCullough, R., Ong, L., & Ramirez, M. (2019). *Alternative proteins: The race for market share is on*. McKinsey & Company. Retrieved from https://www.mckinsey.com/industries/agriculture/our-insights/alternative-proteins-the-race-for-market-share-is-on# Accessed January 5, 2020.

Batista, A. P., Portugal, C. A. M., Sousa, I., Crespo, J. G., & Raymundo, A. (2005). Accessing gelling ability of vegetable proteins using rheological and fluorescence techniques. *International Journal of Biological Macromolecules, 36*(3), 135–143. https://doi.org/10.1016/j.ijbiomac.2005.04.003

Cornet, S. H. V., Snel, S. J. E., Schreuders, F. K. G., Van der, R. G. M., Beyrer, M., & van der Goot, A. J. (2021). Thermo-mechanical processing of plant proteins using shear cell and high-moisture extrusion cooking. *Critical Reviews in Food Science and Nutrition*. https://doi.org/10.1080/10408398.2020.1864618

Dekkers, B. L., Emin, M. A., Boom, R. M., & van der Goot, A. J. (2018). The phase properties of soy protein and wheat gluten in a blend for fibrous structure formation. *Food Hydrocolloids, 79*, 273–281. https://doi.org/10.1016/j.foodhyd.2017.12.033

Emin, M. A., Quevedo, M., Wilhelm, M., & Karbstein, H. P. (2017). Analysis of the reaction behavior of highly concentrated plant proteins in extrusion-like conditions. *Innovative Food Science & Emerging Technologies, 44*, 15–20. https://doi.org/10.1016/j.ifset.2017.09.013

Ersch, C., ter Laak, I., van der Linden, E., Venema, P., & Martin, A. (2015). Modulating fracture properties of mixed protein systems. *Food Hydrocolloids, 44*, 59–65. https://doi.org/10.1016/j.foodhyd.2014.09.009

Ewoldt, R. H., Hosoi, A. E., & McKinley, G. H. (2008). New measures for characterizing nonlinear viscoelasticity in large amplitude oscillatory shear. *Journal of Rheology, 52*(6), 1427–1458. https://doi.org/10.1122/1.2970095

Ewoldt, R. H., & McKinley, G. H. (2017). Mapping thixo-elasto-visco-plastic behavior. *Rheologica Acta, 56*(3), 195–210. https://doi.org/10.1007/s00397-017-1001-8

Ewoldt, R. H., Winter, P., Maxey, J., & McKinley, G. H. (2010). Large amplitude oscillatory shear of pseudoplastic and elastoviscoplastic materials. *Rheologica Acta, 49*(2), 191–212. https://doi.org/10.1007/s00397-009-0403-7

Genovese, D. B., & Rao, M. A. (2003). Vane yield stress of starch dispersions. *Journal of Food Science, 68*(7), 2295–2301. https://doi.org/10.1111/j.1365-2621.2003.tb05762.x

Grabowska, K. J., Tekidou, S., Boom, R. M., & van der Goot, A.-J. (2014). Shear structuring as a new method to make anisotropic structures from soy–gluten blends. *Food Research International, 64*, 743–751. https://doi.org/10.1016/j.foodres.2014.08.010, 0.

Hamann, D., & MacDonald, G. (1992). Rheology and texture properties of surimi and surimi-based foods. In T. C. Lanier, & C. M. Lee (Eds.), *Surimi technology* (pp. 429–500). Marcel Dekker.

Hyun, K., Wilhelm, M., Klein, C. O., Cho, K. S., Nam, J. G., Ahn, K. H., et al. (2011). A review of nonlinear oscillatory shear tests: Analysis and application of large amplitude oscillatory shear (Laos). *Progress in Polymer Science, 36*(12), 1697–1753. https://doi.org/10.1016/j.progpolymsci.2011.02.002

Jones, O. G. (2016). Recent advances in the functionality of non-animal-sourced proteins contributing to their use in meat analogs. *Current Opinion in Food Science, 7*, 7–13. https://doi.org/10.1016/j.cofs.2015.08.002

Klost, M., Brzeski, C., & Drusch, S. (2020). Effect of protein aggregation on rheological properties of pea protein gels. *Food Hydrocolloids, 108*, 106036. https://doi.org/10.1016/j.foodhyd.2020.106036

Lam, A. C. Y., Can Karaca, A., Tyler, R. T., & Nickerson, M. T. (2018). Pea protein isolates: Structure, extraction, and functionality. *Food Reviews International, 34*(2), 126–147. https://doi.org/10.1080/87559129.2016.1242135

Mattice, K. D., & Marangoni, A. G. (2020). Evaluating the use of zein in structuring plant-based products. *Current Research in Food Science, 3*, 59–66. https://doi.org/10.1016/j.crfs.2020.03.004

Moreno, H. M., Domínguez-Timón, F., Díaz, M. T., Pedrosa, M. M., Borderías, A. J., & Tovar, C. A. (2020). Evaluation of gels made with different commercial pea protein isolate: Rheological, structural and functional properties. *Food Hydrocolloids, 99*, 105375. https://doi.org/10.1016/j.foodhyd.2019.105375

Nashif, A., Jones, D., & Henderson, J. (1985). *Vibration damping*. John Wiley.

O'Kane, F. E., Happe, R. P., Vereijken, J. M., Gruppen, H., & Van Boekel, M. A. J. S. (2004). Heat-induced gelation of pea legumin: Comparison with soybean glycinin. *Journal of Agricultural and Food Chemistry, 52*(16), 5071–5078. https://doi.org/10.1021/jf035215h

Pipkin, A. C. (1972). Lectures on viscoelasticity theory. *Applied Mathematical Sciences, 7.* Springer.

Precha-Atsawanan, S., Uttapap, D., & Sagis, L. M. C. (2018). Linear and nonlinear rheological behavior of native and debranched waxy rice starch gels. *Food Hydrocolloids, 85*, 1–9. https://doi.org/10.1016/j.foodhyd.2018.06.050

Ptaszek, P. (2014). Large amplitudes oscillatory shear (Laos) behavior of egg white foams with apple pectins and xanthan gum. *Food Research International, 62*, 299–307. https://doi.org/10.1016/j.foodres.2014.03.002

Samard, S., & Ryu, G. H. (2019). A comparison of physicochemical characteristics, texture, and structure of meat analogue and meats. *Journal of the Science of Food and Agriculture, 99*(6), 2708–2715. https://doi.org/10.1002/jsfa.9438

Schreuders, F. K. G., Bodnar, I., Erni, P., Boom, R. M., & Goot, A. J. Van Der (2020). Water redistribution determined by time domain NMR explains rheological properties of dense fibrous protein blends at high temperature. *Food Hydrocolloids, 101*, 105562. https://doi.org/10.1016/j.foodhyd.2019.105562

Schreuders, F. K. G., Dekkers, B. G., Bodnár, I., Erni, P., Boom, R., & van der Goot, A. (2019). Comparing structuring potential of pea and soy protein with gluten for the preparation of meat analogues. *Journal of Food Engineering, 261*, 32–39. https://doi.org/10.1016/j.jfoodeng.2019.04.022

Schreuders, F. K. G., Sagis, L. M. C., Bodnár, I., Erni, P., Boom, R. M., & van der Goot, A. J. (2021). Small and large oscillatory shear properties of concentrated proteins. *Food Hydrocolloids, 110*, 106172. https://doi.org/10.1016/j.foodhyd.2020.106172

Shand, P. J., Ya, H., Pietrasik, Z., & Wanasundara, P. K. J. P. D. (2008). Transglutaminase treatment of pea proteins: Effect on physicochemical and rheological properties of heat-induced protein gels. *Food Chemistry, 107*(2), 692–699. https://doi.org/10.1016/j.foodchem.2007.08.095

Shewry, P. R., & Tatham, A. S. (1997). Disulphide bonds in wheat gluten proteins. *Journal of Cereal Science, 25*(3), 207–227. https://doi.org/10.1006/jcrs.1996.0100

Szopinski, D., & Luinstra, G. A. (2016). Viscoelastic properties of aqueous guar gum derivative solutions under large amplitude oscillatory shear (Laos). *Carbohydrate Polymers, 153*, 312–319. https://doi.org/10.1016/j.carbpol.2016.07.095

Tao, R., Rice, K. D., Djakeu, A. S., Mrozek, R. A., Cole, S. T., Freeney, R. M., et al. (2019). Rheological characterization of next-generation ballistic witness materials for body armor testing. *Polymers, 11*(3), 447. https://doi.org/10.3390/polym11030447

Truong, V. D., & Daubert, C. R. (2000). Comparative study of large strain methods for assessing failure characteristics of selected food gels. *Journal of Texture Studies, 31*(3), 335–353. https://doi.org/10.1111/j.1745-4603.2000.tb00294.x

Truong, V. D., & Daubert, C. R. (2001). Textural characterization of cheeses using vane rheometry and torsion analysis. *Journal of Food Science, 66*(5), 716–721. https://doi.org/10.1111/j.1365-2621.2001.tb04627.x

Tunick, M. H., & Van Hekken, D. L. (2010). Rheology and texture of commercial queso fresco cheeses made from raw and pasteurized milk. *Journal of Food Quality, 33*(suppl. 1), 204–215. https://doi.org/10.1111/j.1745-4557.2010.00331.x

Wereley, N. M., Chaudhuri, A., Yoo, J. H., John, S., Kotha, S., Suggs, A., et al. (2006). Bidisperse magnetorheological fluids using Fe particles at nanometer and micron scale. *Journal of Intelligent Material Systems and Structures, 17*(5), 393–401. https://doi.org/10.1177/1045389X06056953

Zhou, L., Cook, L. P., & McKinley, G. H. (2010). Probing shear-banding transitions of the VCM model for entangled wormlike micellar solutions using large amplitude oscillatory shear (Laos) deformations. *Journal of Non-newtonian Fluid Mechanics, 165*(21–22), 1462–1472. https://doi.org/10.1016/j.jnnfm.2010.07.009